coatings

MDPI

Article

Enhanced Photocatalytic Activity of the Cu_2SnS_3 + GO Composite for the Degradation of Navy Blue ME2RL Industrial Dye

Harshad D. Shelke [1], Archana R. Machale [2], Avinash A. Surwase [3], Shoyebmohamad F. Shaikh [4], Abu ul Hassan S. Rana [5] and Habib M. Pathan [1,*]

[1] Advanced Physics Laboratory, Department of Physics, Savitribai Phule Pune University, Pune 411007, India
[2] Solid State Physics Laboratory, Department of Physics, Yashwantrao Chavan Institute of Science Satara, Satara 415001, India
[3] Rayat Institute of Research and Development, Shivaji University Kolhapur, Satara 415001, India
[4] Department of Chemistry, College of Science, King Saud University, Riyadh 11451, Saudi Arabia
[5] Department of Electrical and Electronic Engineering, The University of Melbourne, Parkville 3010, Australia
* Correspondence: habib.pathan@gmail.com

Abstract: In the present work, the photocatalytic activity of pristine Cu_2SnS_3 (CTS) and a composite with graphene oxide (GO), i.e., CTS + GO, prepared by the precipitation technique, and its utilization as a catalyst for the degradation of Navy Blue (NB) ME2RL reactive azo dye were studied. The structural, morphological, and optical properties of the synthesized composite were evaluated. The degradation of azo dyes was used to evaluate the photocatalytic activity of the CTS + GO composite under visible light irradiation. When compared to pure CTS, the CTS + GO nanocomposite demonstrated increased photocatalytic activity. The improved photocatalysis is due to reduced recombination of generated charge carriers, better visible light absorption, and modified dye absorption via GO amalgamation in CTS. The simple and well-organized chemical bath method for catalyst preparation will be more suited to industrial production.

Keywords: Cu_2SnS_3; GO; nanocomposite; NB ME2RL; photocatalyst

check for updates

Citation: Shelke, H.D.; Machale, A.R.; Surwase, A.A.; Shaikh, S.F.; Rana, A.u.H.S.; Pathan, H.M. Enhanced Photocatalytic Activity of the Cu_2SnS_3 + GO Composite for the Degradation of Navy Blue ME2RL Industrial Dye. *Coatings* **2023**, *13*, 522. https://doi.org/10.3390/coatings13030522

Academic Editor: Maria Vittoria Diamanti

Received: 29 January 2023
Revised: 16 February 2023
Accepted: 20 February 2023
Published: 26 February 2023

Copyright: © 2023 by the authors. Licensee MDPI, Basel, Switzerland. This article is an open access article distributed under the terms and conditions of the Creative Commons Attribution (CC BY) license (https://creativecommons.org/licenses/by/4.0/).

1. Introduction

Water pollution has become a very serious ecological problem worldwide. Water pollution is mainly caused by various contaminants, such as heavy metals, natural organic materials, and microorganisms, etc. [1]. These pollutants originate from the textile, agriculture, and pharmaceutical industries. Industrial waste is fraught with several harmful pollutants for human health and the environment [2]. Therefore, it is necessary to remove hazardous pollutants before they are discharged into fresh water. For the treatment of wastewater, a variety of traditional techniques including physical, chemical, and biological methods have been applied. Cheaper and less time-consuming processes are the major tools for accessing safe water. Unfortunately, however, these methods have many limitations, such as low efficiency, high operating cost, and a long time requirement for the removal of dyes and non-biodegradable end products; hence, they require post-treatments [3]. Therefore, advanced oxidation processes (AOPs) have received much attention from researchers to deal with the purification of wastewater. Similar to all dyes that can be oxidized, AOPs have many advantages, including non-selectivity and quick processing [4]. Photocatalysis, a process where light derives a catalytic activity, generally has two categories, namely heterogeneous and homogeneous photocatalysis [5]. Between these, heterogeneous photocatalysis can be used for the degradation of various organic pollutants in wastewater [6]. Because of its capacity to generate biodegradable and nontoxic end products via a facile, simple, unique, and green process, photocatalysis has been a center of attention in the

realm of research and development [7]. In photocatalysis processes, semiconductor-based photocatalysts have been widely utilized in the treatment of wastewater contaminated with different environmental pollutants [8]. Among the available functional materials, copper-based ternary sulfides are important because of their narrow band gaps and high absorption coefficients [9]. Recently, copper tin sulfide, i.e., Cu_2SnS_3 (CTS) has gained extensive attention due to its possible application in photocatalysis. CTP, a ternary chalcogenide and a p-type semiconductor, has a high absorption coefficient (>10^4 cm^{-1}) and a band gap of 1.3–1.6 eV [10]. As the CTS's component parts are benign and abundant on Earth, they can be used to effectively photodegrade dye, which is an environmentally and economically friendly process. Also, graphene oxide (GO) shows electronic properties and exceptional crystals which have already emerged as a photocatalytic material due to its adsorption capability, charge transfer, and higher surface area [11].

Consequently, loading graphene sheets on the surface of metal sulfide semiconductor materials could greatly enhance their photocatalytic activity [12]. L. Zou et al. reported on the degradation of Congo Red dye molecules in the presence of a cadmium sulfide-reduced graphene oxide photocatalyst and determined the greatest photocatalytic efficiency to be approximately 90% in 4 h [13]. Das et al. studied the hydrothermal synthesis of NiS_2-rGO nanocomposite materials and how well they broke down CR dye molecules when exposed to sunlight. The photocatalytic studies demonstrated outstanding efficiency, with up to 76.5% in 240 min and 86.9% in 50 min of visible light irradiation for methyl orange (MO) and Cr (VI), respectively [14]. Vladimir E. Fedorov et al. found that the produced nanocomposite acted as an excellent photocatalyst toward the diazo Congo Red (CR) dye molecule when exposed to the irradiation of natural sunlight, with a maximum degradation efficiency of 98.76% [15].

In the present work, we employed the room temperature and simple precipitation technique (PT) to fabricate pristine CTS and CTS + GO composites for the degradation of Navy Blue (NB) ME2RL reactive azo dye under visible light irradiation. To our knowledge, this is the first report on the degradation of NB dye using CTS as a photocatalyst. However, the influence of GO in tuning the characteristics of CTS was methodically researched, and an appropriate photocatalytic mechanism is discussed.

2. Experimental Details

2.1. Materials

The following chemicals were used in the preparation of CTS and CTS + GO. Cuprous chloride (CuCl, 99.90%, Sigma Aldrich, Mumbai, India), stannic chloride ($SnCl_4$, 99.85%, SRL, Mumbai, India), sodium thiosulfate ($Na_2S_2O_3$, 99.99%, SRL, Mumbai, India), and NB ME2RL reactive azo dye were used.

2.2. Preparation of Photocatalyst

For CTS nanoparticles synthesis, analytical reagent (AR) grade chemicals and solutions were used. Typically, 0.1 M CuCl, 0.05 M $SnCl_4$, and 0.2 M $Na_2S_2O_3$ were dissolved in 50 mL of double distilled water (DDW) under continuous magnetic stirring for 30 min. The mixture solution was placed in a 50 mL beaker and placed at room temperature for 2 h with continuous stirring. After the completion of the reaction, the precipitate was removed, rinsed several times with DDW, and dried overnight at 80 °C. Finally, it was annealed for 1 h at 450 °C in a sulfur atmosphere to obtain the pure phase of CTS. The initial pH of the solution was approximately 3. The resulting CTS nanoparticles were blackish in colour. The purchased GO powder (10 mg) was dispersed into the DDW and influenced with the prepared sample with vigorous stirring.

2.3. Characterization Techniques

X-ray diffraction (XRD) was used to measure the crystallite size of pure CTS and the CTS + GO composite (model: XRD, Rigaku "D/B max 2400", Cu Ka = 0.154 nm Akishima, Japan). Scanning electron microscopy was used to determine the morphology of the synthe-

sized material (model: JEOL-JSM 6360-A, Austin, TX, USA). Both the optical properties and the photocatalytic activity were evaluated using a UV-Visible spectrophotometer (model: JASCO V-670, Via Luigi Cadorna, Cremella LC, Italy). To estimate the Brunauer–Emmett–Teller surface area and pore size, a Micromeritics surface area analyzer instrument (ASAP 2020, GA 30093-2901, Norcross, GA, USA) was used, and the powder sample was vacuum degassed for 18 h at 200 °C to remove the surface adsorbed gases and contaminates if any. For analysis purposes, liquid Nit Austin, Texas, USA rogen (LN2) was utilized to maintain the temperature of 77 K.

2.4. Photocatalytic Activity of CTS Nanoparticles

The NB ME2RL azo dye was first produced as a 50 mL aqueous solution with a concentration of 1×10^{-5} M at room temperature. Afterwards, the dye solution was made and 2 mg of pure CTS and CTS + GO photocatalyst powder were added. The solution was magnetically agitated and left in the dark for 5 h prior to irradiation to achieve adsorption-desorption equilibrium. The catalyst was exposed to a 300 W xenon lamp. The absorbance spectrum of this produced dye solution in both the absence and presence of a photocatalyst was recorded using the UV-Visible Spectrophotometer. While the solution was degrading, it was constantly stirred. Consequently, 3 mL of the solution was pipetted out every 60 min, and the solution was centrifuged to get rid of the photocatalyst precipitate. The NB ME2RL dye concentration was noted. The procedure was continued up until the point of maximum deterioration.

3. Results and Discussion

3.1. Structural Analysis

X-ray diffraction was utilized to carry out a structural examination of the samples that were prepared. The XRD patterns of GO, CTS, and CTS + GO are shown in Figure 1. In Figure 1a, the characteristic peak of GO is found at 2θ = 10.06° and 42.54° with hkl planes of (001) and (100), respectively [16]. Figure 1b shows the XRD pattern of the pristine CTS material, and Figure 1c shows the XRD pattern of the CTS + GO composite material. The distinctive peaks of CTS + GO with their corresponding planes are 2θ = 28.73° (plane 112), 47.95° (plane 220) and 56.89° (plane 312), indicating the tetragonal phase (JCPDS: 01-089-4714) of the prepared CTS + GO [17]. Apart from the CTS peaks, a small peak appeared at 2θ = 31.87°, indicating a minor Cu_2S phase. The intensity of the typical diffraction peak in the CTS + GO composite gradually decreases in comparison to pristine CTS. It demonstrates how the use of graphene limits the creation of CTS particles with high crystallinities. As a result, a lot of active catalytic sites can be supplied by the CTS particles created between graphene layers. Moreover, the composite does not exhibit the graphene (001) peak, demonstrating the absence of graphene particle stacking [18]. The particle size of the pristine CTS and CTS + GO composite was estimated using Scherrer's equation (Equation (1)).

$$D = \frac{K\lambda}{\beta \cos\theta} \quad (1)$$

where K is shape factor, D is the average crystallite size, β is FWHM in radians, λ is wavelength, and θ is the Bragg angle of the peak in radians. The average crystallite sizes of the CTS and CTS + GO composite were calculated to be 54.32 and 48.96 nm, respectively.

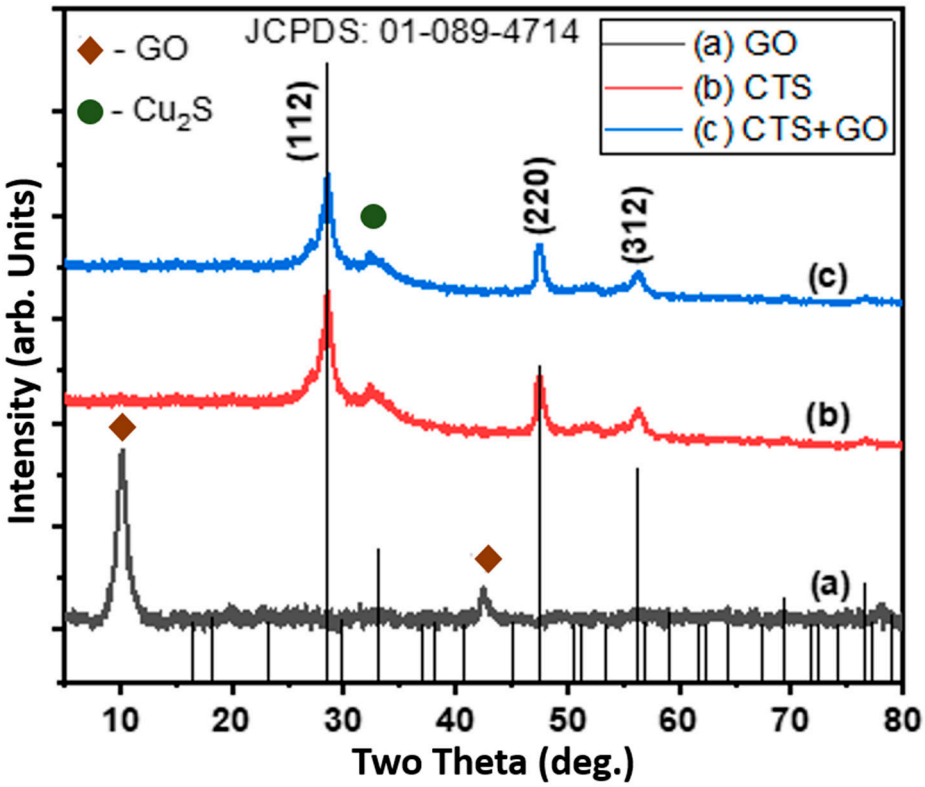


Figure 1. X-ray diffraction patterns of (**a**) GO, (**b**) CTS, and (**c**) CTS + GO materials.

3.2. Morphological Analysis

SEM analysis of the CTS and CTS + GO composites was used to examine the surface morphology of the synthesized material, as depicted in Figure 2. Illustrated in Figure 2A, the SEM image of pristine CTS revealed that the particles were aggregated and crystalline in shape. The SEM image of the CTS + GO composite is displayed in Figure 2C, which revealed that the reduction and compositing processes had completely destroyed the GO's layered structure, leaving just a little sheet-like structure in the backdrop [19]. Moreover, the CTS nanoparticles' tendency to aggregate was lessened as a result of the inclusion of GO. This might be as a result of an increase in the amount of surface area accessible for GO and nanoparticle interaction, which results in a quality enhancement in the nanoparticles' surface passivation [20]. As shown in Figure 2B, the EDX spectrum of virgin CTS revealed that the material's composition of Cu, Sn, and S was 2.3:1:3.1, which was consistent with the elements' predicted stoichiometric ratio. The CTS + GO composite's EDX spectrum is displayed in Figure 2D. The composite's distribution of the elements carbon (C), oxygen (O), copper (Cu), tin (Sn), and sulfur (S) is displayed. The micrographs' consistent distribution of each component supports the uniform distribution of the nanoparticles with GO nanoparticles [21]. The existence of these elements in the produced composite is also confirmed by the EDX of CTS + GO (Figure 2D).

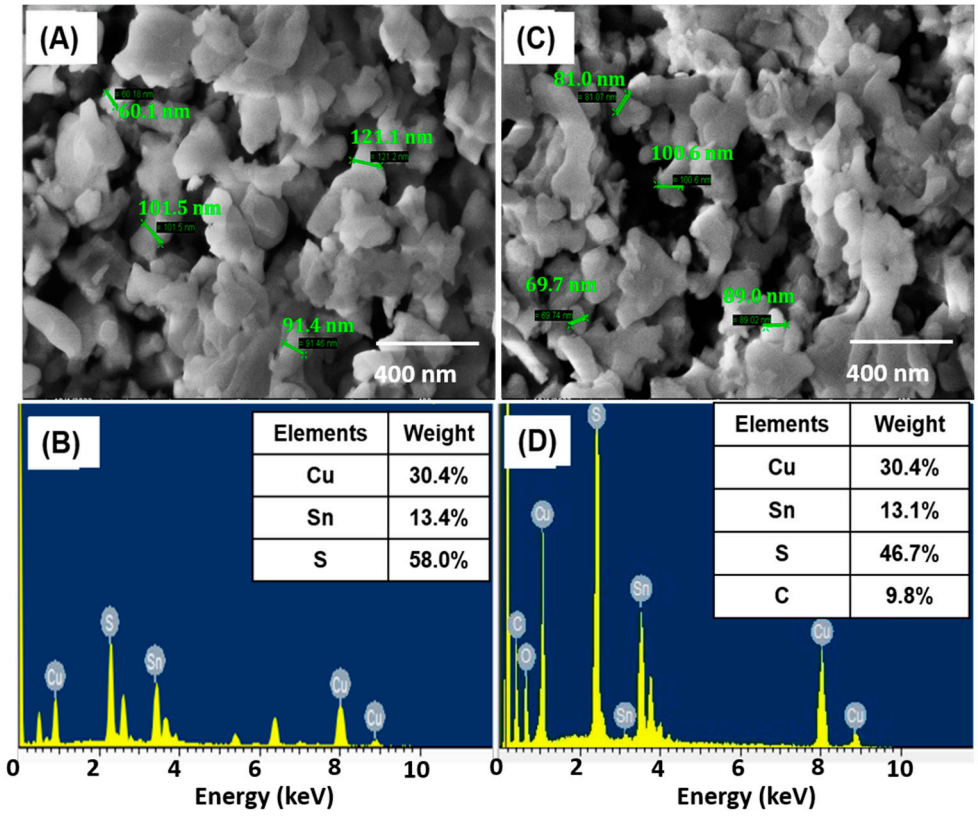


Figure 2. SEM images and EDX spectra of (**A**,**B**) pristine CTS and (**C**,**D**) CTS + GO material.

3.3. Brunauer-Emmett-Teller (BET) Analysis

When characterizing novel porous materials, one of the most significant characteristics to consider is the surface area of the material. Brunauer-Emmett-Teller (BET) analysis is a common method used to determine the specific surface area of materials, particularly porous solids. The BET method involves measuring the quantity of gas molecules adsorbed onto a material at different pressures, typically using nitrogen gas as the adsorbate. The data is then analyzed using the BET equation, which relates the quantity of adsorbed gas to the surface area of the material. Figure 3A,B show the nitrogen adsorption isotherm curves and pore size distribution calculations through the Barrett-Joyner-Halenda (BJH) method from the desorption branch of CTS and CTS + GO, respectively. From Figure 3A, it is clear that the pristine CTS material shows 4.38 $m^2\ g^{-1}$ and the CTS + GO composite shows 13.91 $m^2\ g^{-1}$ specific surface area. Hence, it is concluded that the composite material shows a 1.7-fold higher value than the pristine material. The uniform distribution of pore size was evaluated by the BJH method, as illustrated in Figure 3B. The values are determined to be 0.00153 $cm^3\ g^{-1}$ and 0.003519 $cm^3\ g^{-1}$ for pristine CTS and the CTS + GO composite, respectively. The increase in both parameters is related to the wt.% of GO with the CTS [22]. The CTS + GO composite shows a higher surface area and pore size than the pristine CTS sample, which would act as a better photocatalyst.

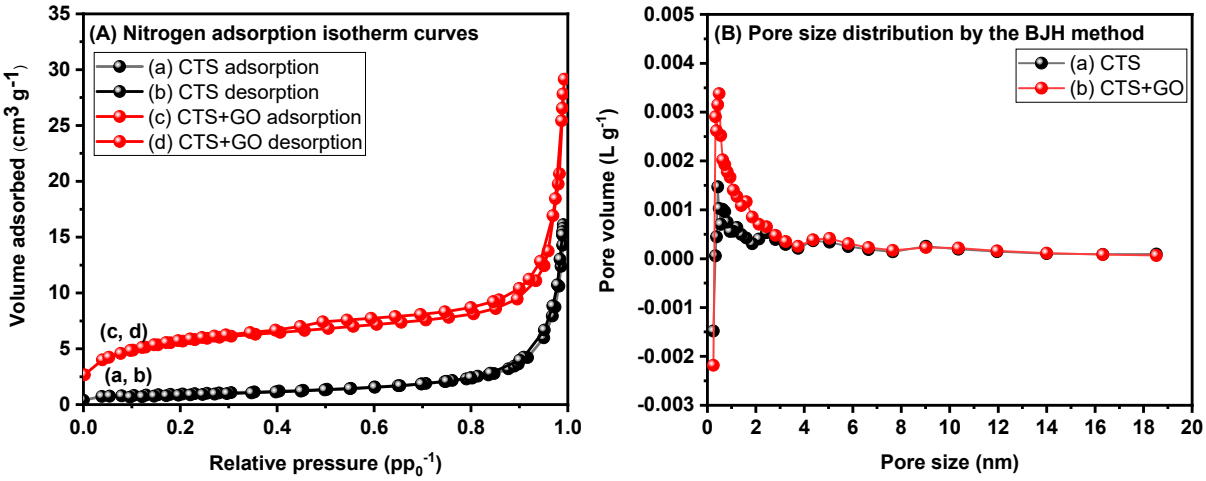


Figure 3. (**A**) Nitrogen adsorption isotherm curves and (**B**) pore size distribution calculated by the BJH method from the desorption branch of CTS and CTS + GO material.

3.4. Optical Analysis

The absorbance spectra of the pure CTS thin material and the CTS + GO thin material were examined by a UV-Visible spectrophotometer throughout a wavelength range of 400–1000 nm, and the results are depicted in Figure 4A. After the incorporation of GO, the optical absorption edge moved to longer wavelengths, as seen in Figure 4A. This change was brought about by the presence of GO. The energy band gap values were calculated using Tauc's equation. Figure 4B shows that the band gap values of the pristine and GO composite samples were 1.40 eV and 1.35 eV, respectively. A similar phenomenon was also reported by S. Yao et al. [23]. The drop in band gap energy might be a consequence of the development of sub-band states amongst the valence band and conduction band of CTS by the incorporation of GO [20]. The composite effect shows a decrease in the band gap of CTS, which is in good agreement with CTS acting as a better photocatalyst.

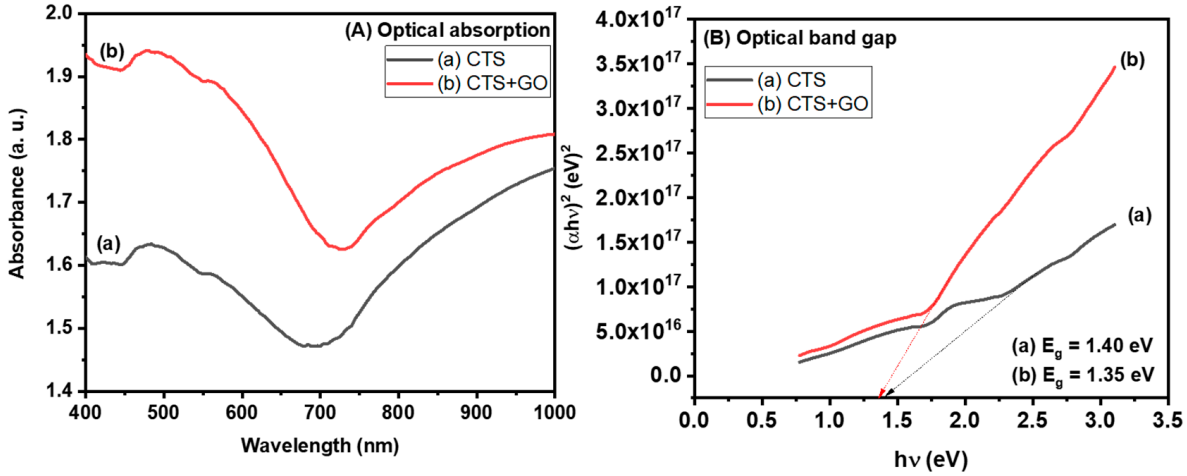


Figure 4. (**A**) Optical absorption spectra and (**B**) band gap spectra of CTS and CTS + GO material.

3.5. Photocatalytic Activity

The examination of NB ME2RL reactive azo dye degradation using the CTS + GO catalyst was performed under a xenon lamp as the visible light source. The spectrum of photocatalytic dye degradation is shown in Figure 5. Before irradiation, 2 mg of catalyst was mixed into the dye solution with 30 min of stirring and then kept in the dark for 5 h

to obtain an adsorption-desorption equilibrium [24]. Before irradiation, the absorption spectrum of the prepared solution was recorded and specified by the 0 min reading in Figure 5. The absorption peak at 600 nm was taken as a reference. The peak of the dye did not degrade in the absence of light even when the photocatalyst was added. After being exposed to visible light, the solution's absorption spectra were recorded by taking 3 mL out of the solution after every 60 min. To extract the sample, the pipette mixture was centrifuged. The synchronic UV-Visible spectrometer 119 (Ahmedabad, Gujarat, India) was used to record the spectra each time. It is clear from Figure 5 that the absorbance of the NB ME2RL azo dye decreased with the addition of a catalyst. The photodegradation rate constant of the CTS + GO composite sample was faster than that of the pristine CTS sample. The results were attributed to the combined effects of enhanced visible light absorption by GO and efficient charge separation due to CTS in the photocatalyst system [25]. The dye degradation efficacy was calculated via the following:

$$\text{The degradation efficiency } (\%) = \left[\frac{(A_0 - A_t)}{A_0}\right] \times 100 \quad (2)$$

where A_0 and A_t are the initial absorbance of NB ME2RL azo dye without any catalyst and the dye solution absorption with a catalyst, respectively. Figure 5A shows that the activity of dye degradation of pristine CTS nanoparticles is 79% for NB ME2RL dye in 240 min. The dye becomes degraded and colorless after the addition of the catalyst.

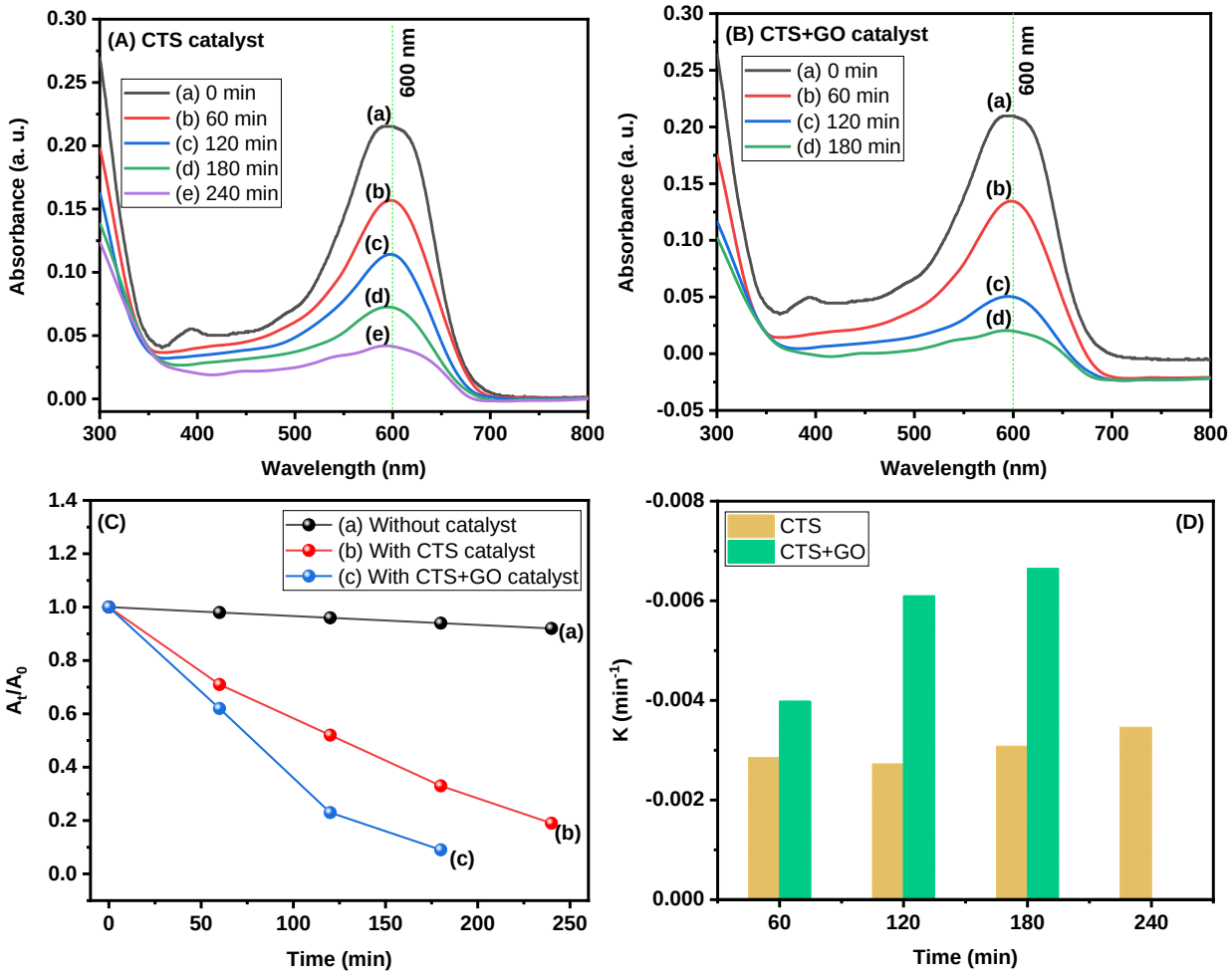


Figure 5. UV-Visible absorption spectra of NB ME2RL dye degradation with (**A**) pristine CTS and (**B**) CTS + GO composite; (**C**) plot of [At]/[A0] as a function of radiation time for CTS and CTS + GO materials and (**D**) bar diagram of 'K' vs. radiation time for CTS and CTS + GO materials.

Figure 5B shows that the activity of dye degradation of the CTS + GO composite is 88% for NB ME2RL azo dye in 180 min. The presence of GO in the CTS + GO composite material enhances the surface area and increases photon charge carriers to degrade the NB ME2RL dye, as depicted in Figure 5B [26]. The $[A_t/A_0]$ vs. time graph depicts the dye degradation in the presence/absence of the photocatalyst, as portrayed in Figure 5C. The results clearly show a significant change in the degradation efficiency according to the addition of GO. The following equation was used to determine the rate constant of the first-order kinetic reaction 'k_{app}':

$$ln\left(\frac{A_0}{A_t}\right) = -k_{app}t \quad (3)$$

The values of 'k_{app}' for the pristine CTS and CTS + GO composite samples are found to be 6.16×10^{-3} min^{-1} and 1.13×10^{-3} min^{-1}, respectively, which obeys the first-order kinetic reaction. Similarly, the following equation was used to compute the catalyst's activity parameter:

$$k = \frac{k_{app}}{m} \quad (4)$$

where 'm' is the mass of the catalyst. The activity parameter 'k' for both photocatalyst samples was calculated as 3.08×10^{-4} min^{-1} g^{-1} and 6.65×10^{-4} min^{-1} g^{-1}, respectively. Figure 5D shows the 'k' bar graph for both composite and pristine samples. From the graph, it is seen that the 'k' value for the composite CTS + GO sample is greater than that for the pristine CTS sample.

3.6. Photocatalytic Process Mechanism

The mechanism of photocatalytic degradation for the CTS + GO composite material is shown in Figure 6. After adding GO, the photocatalytic activity of this composite has an augmentation, which is mainly due to GO, which can act as an electron conductor to promote the migration of the photogenerated charge carriers [22]. It is evident that the photogenerated electrons may appear more effective when exposed to visible light:

$$CTS + GO + hv \rightarrow h+ + e^- \quad (5)$$

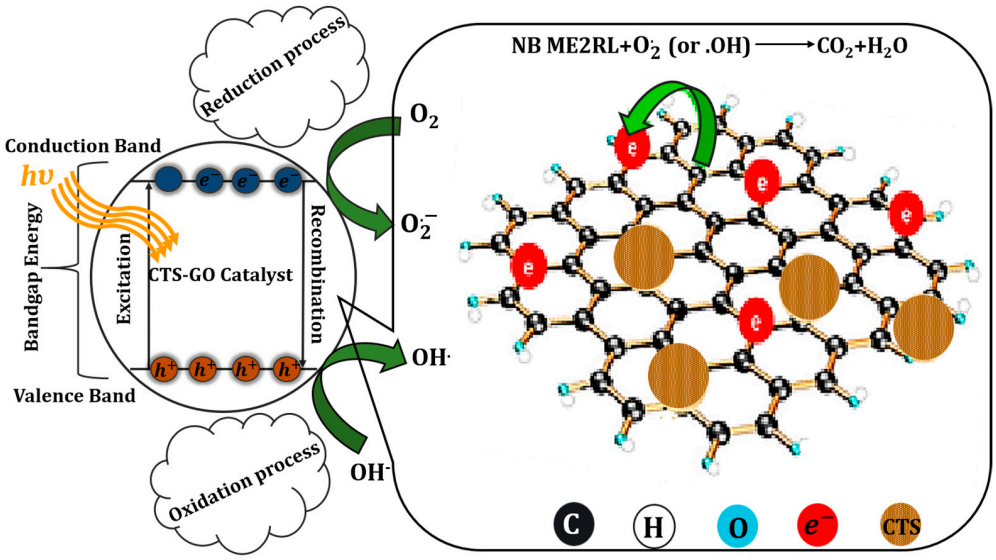


Figure 6. Schematic illustration of photocatalytic degradation of NB ME2RL dye over the CTS + GO composite in the presence of visible light.

In CTS + GO, the excited electrons leave holes (h+) in the valence band (VB) by hopping from VB to the conduction band (CB). The GO may compose and elate the generated electrons. The method will effectively disperse the photogenerated e-h pairs and extend the life of the charge carriers. The surface-absorbed O_2 on the GO can be reduced by the photogenerated e to produce $\cdot O_2^-$ radicals, and additional active species such as $\cdot HO_2$ of ·OH radicals can also be produced, as shown in the following reactions.

$$e^- + O_2 \rightarrow \cdot O_2^- \quad (6)$$

$$O_2^- + H_2O \rightarrow \cdot HO_2 + OH^- \quad (7)$$

$$2 \cdot HO_2 \rightarrow H_2O_2 + O_2 \quad (8)$$

$$H_2O_2 + e^- \rightarrow \cdot OH + OH^- \quad (9)$$

The $\cdot O_2^-$ and ·OH radicals can photodegrade the NB ME2RL molecules, converting them to CO_2, H_2O, and other mineralization byproducts. Similar to this, hydroxyl radicals (OH) produced by the photogenerated h+ can likewise react with HO^- produced by the H_2O to oxidize the absorbed NB on the catalyst surface. As a result, NB can degrade capably when illuminated by visible light:

$$h+ + H_2O \rightarrow \cdot OH + H^+ \quad (10)$$

$$O_2^-, \cdot OH + NB \rightarrow CO_2 + H_2O \quad (11)$$

It is also reported that the GO sheets might prevent photocorrosion of the composite nanoparticles [27]. The interface migration of the photogenerated carriers are further facilitated by the GO nanosheets. It can make a competent separation of the photogenerated holes and electrons, in that way reducing the recombination possibility of photogenerated carriers, avoiding the photooxidation of CTS by holes, and enhancing the stability and photocatalytic activity. Therefore, the performance of photocatalytic degradation can be enhanced greatly [28].

4. Conclusions

The photocatalytic activity of the pristine CTS and CTS + GO composite materials prepared by a simple and economic PT route was explored for the degradation of NB ME2RL reactive azo dye. The photocatalyst activity was enhanced under visible light illumination with the incorporation of GO into the CTS material. After the incorporation of GO into CTS, the band gap energy was reduced. The band gap values were found to be 1.43 eV and 1.31 eV for the pristine CTS and CTS + GO composite materials, respectively. The greater photocatalytic activity of the composite material can be attributed to the presence of GO in the CTS, which enhances electron conductivity and creates a large number of active sites. A 79% degradation of the NB ME2RL azo dye was obtained under visible light irradiation for pristine CTS. The incorporation of GO plays a vibrant role in the ideal catalytic activity, because photogenerated electrons can be rapidly transferred to GO sheets, whereas GO commonly acts as an electron acceptor and allocates channels in composites. Due to the incorporation of GO, the degradation efficiency was enhanced by up to 88% for the NB ME2RL azo dye. This easy and green PT route for the synthesis of catalysts is more relevant to industrial manufacturing.

Author Contributions: Conceptualization, H.D.S., A.R.M. and A.A.S.; methodology, H.D.S., A.R.M. and H.M.P.; software, A.u.H.S.R.; validation, H.M.P. and S.F.S.; formal analysis, A.R.M. and A.A.S.; investigation, H.D.S.; resources, H.M.P. and S.F.S.; data curation, A.u.H.S.R.; writing—original draft preparation, H.D.S., A.R.M. and A.A.S.; writing—review and editing, H.M.P., A.u.H.S.R. and S.F.S.; visualization, A.R.M.; supervision, H.M.P.; project administration, H.M.P. and S.F.S.; funding acquisition, H.M.P. and S.F.S. All authors have read and agreed to the published version of the manuscript.

Funding: The authors are thankful to the Researchers Supporting Project number (RSP2023R370), King Saud University, Riyadh, Saudi Arabia for funding this project.

Institutional Review Board Statement: Not applicable.

Informed Consent Statement: Not applicable.

Data Availability Statement: The data presented in this study are available on request to the corresponding author.

Acknowledgments: The authors extend their sincere appreciation to the Researchers Supporting Project number (RSP2023R370), King Saud University, Riyadh, Saudi Arabia for funding support.

Conflicts of Interest: The authors declare no conflict of interest.

References

1. Zhang, Z.; Li, J.; Wang, H.; Li, Y.; Duan, X. Impact of co-contamination by PAHs and heavy metals on micro-ecosystem in bioretention systems with soil, sand, and water treatment residuals. *J. Clean. Prod.* **2023**, *383*, 135417. [CrossRef]
2. Mandeep; Gupta, G.K.; Liu, H.; Shukla, P. Pulp and paper industry-based pollutants, their health hazards and environmental risks. *Curr. Opin. Environ. Sci. Health* **2019**, *12*, 48–56. [CrossRef]
3. Lin, C.; Liu, H.; Guo, M.; Zhao, Y.; Su, X.; Zhang, P.; Zhang, Y. Plasmon-induced broad spectrum photocatalytic overall water splitting: Through non-noble bimetal nanoparticles hybrid with reduced graphene oxide. *Colloids Surfaces A Physicochem. Eng. Asp.* **2022**, *646*, 128962. [CrossRef]
4. Lops, C.; Ancona, A.; Di Cesare, K.; Dumontel, B.; Garino, N.; Canavese, G.; Hérnandez, S.; Cauda, V. Sonophotocatalytic degradation mechanisms of rhodamine B dye via radicals generation by micro- and nano-particles of ZnO. *Appl. Catal. B Environ.* **2019**, *243*, 629–640. [CrossRef]
5. Zhang, Y.; Wang, Y.; Guo, C.; Wang, Y. Molybdenum carbide-based photocatalysts: Synthesis, functionalization, and applications. *Langmuir* **2022**, *38*, 12739–12756. [CrossRef] [PubMed]
6. Gaya, U.I.; Abdullah, A.H. Heterogeneous photocatalytic degradation of organic contaminants over titanium dioxide: A review of fundamentals, progress and problems. *J. Photochem. Photobiol. C Photochem. Rev.* **2008**, *9*, 1–12. [CrossRef]
7. Wagh, S.S.; Jagtap, C.V.; Kadam, V.S.; Shaikh, S.F.; Ubaidullah, M.; Pandit, B.; Salunkhe, D.B.; Patil, R.S. Silver doped ZnO nanoparticles synthesized for photocatalysis application. *ES Energy Environ.* **2022**, *17*, 94–105. [CrossRef]
8. Liu, H.; Wang, C.; Wang, G. Photocatalytic advanced oxidation processes for water treatment: Recent advances and perspective. *Chem.—Asian J.* **2020**, *15*, 3239–3253. [CrossRef]
9. Xia, C.; Wu, W.; Yu, T.; Xie, X.; van Oversteeg, C.; Gerritsen, H.C.; de Mello Donega, C. Size-dependent band-gap and molar absorption coefficients of colloidal CuInS2 quantum dots. *ACS Nano* **2018**, *12*, 8350–8361. [CrossRef] [PubMed]
10. Shelke, H.D.; Machale, A.R.; Survase, A.A.; Pathan, H.M.; Lokhande, C.D.; Lokhande, A.C.; Shaikh, S.F.; Rana, A.u.H.S.; Palaniswami, M. Multifunctional Cu_2SnS_3 nanoparticles with enhanced photocatalytic dye degradation and antibacterial activity. *Materials* **2022**, *15*, 3126. [CrossRef] [PubMed]
11. Fu, L.; Li, G.; Shang, C.; Mao, E.; Huang, L.; Wang, X.; Ma, G.; Wang, X.; Zhou, G. Reduced graphene oxide boosted ultrafine Cu_2SnS_3 nanoparticles for high-performance sodium storage. *ChemElectroChem* **2019**, *6*, 2949–2955. [CrossRef]
12. Hu, P.; Liu, X.; Liu, B.; Li, L.; Qin, W.; Yu, H.; Zhong, S.; Li, Y.; Ren, Z.; Wang, M. Hierarchical layered Ni_3S_2-graphene hybrid composites for efficient photocatalytic reduction of Cr(VI). *J. Colloid Interface Sci.* **2017**, *496*, 254–260. [CrossRef]
13. Zou, L.; Wang, X.; Xu, X.; Wang, H. Reduced graphene oxide wrapped CdS composites with enhanced photocatalytic performance and high stability. *Ceram. Int.* **2016**, *42*, 372–378. [CrossRef]
14. Borthakur, P.; Das, M.R. Hydrothermal assisted decoration of NiS_2 and CoS nanoparticles on the reduced graphene oxide nanosheets for sunlight driven photocatalytic degradation of azo dye: Effect of background electrolyte and surface charge. *J. Colloid Interface Sci.* **2018**, *516*, 342–354. [CrossRef]
15. Borthakur, P.; Boruah, P.K.; Darabdhara, G.; Sengupta, P.; Das, M.R.; Boronin, A.I.; Kibis, L.S.; Kozlova, M.N.; Fedorov, V.E. Microwave assisted synthesis of CuS-reduced graphene oxide nanocomposite with efficient photocatalytic activity towards azo dye degradation. *J. Environ. Chem. Eng.* **2016**, *4*, 4600–4611. [CrossRef]
16. Nakate, Y.T.; Sangale, S.S.; Shaikh, S.F.; Shinde, N.M.; Shirale, D.J.; Mane, R.S. Human urine-derived naturally heteroatom doped highly porous carbonaceous material for gas sensing and supercapacitor applications. *Ceram. Int.* **2022**, *48*, 28942–28950. [CrossRef]
17. Sebastian, A.; Maheskumar, V.; Bhuvanesh, N.; Vidhya, B.; Nandhakumar, R.; Jiang, Z. Photocatalytic performance of Cu_3SnS_4 (CTS)/reduced graphene oxide (RGO) composite prepared via ball milling and solvothermal approach. *J. Mater. Sci. Mater. Electron.* **2020**, *31*, 21408–21418. [CrossRef]
18. Liu, H.; Chen, Z.; Jin, Z.; Su, Y.; Wang, Y. A reduced graphene oxide supported Cu_3SnS_4 composite as an efficient visible-light photocatalyst. *Dalt. Trans.* **2014**, *43*, 7491–7498. [CrossRef]

19. Vadivel, S.; Maruthamani, D.; Paul, B.; Dhar, S.S.; Habibi-Yangjeh, A.; Balachandran, S.; Saravanakumar, B.; Selvakumar, A.; Selvam, K. Biomolecule-assisted solvothermal synthesis of Cu_2SnS_3 flowers/RGO nanocomposites and their visible-light-driven photocatalytic activities. *RSC Adv.* **2016**, *6*, 74177–74185. [CrossRef]
20. Olatunde, O.C.; Onwudiwe, D.C. Synthesis of reduced graphene oxide/copper tin sulfide (Cu_2SnS_3) composite for the photocatalytic degradation of tetracycline. *J. Inorg. Organomet. Polym. Mater.* **2022**, *32*, 2578–2590. [CrossRef]
21. Tao, H.-C.; Zhu, S.-C.; Yang, X.-L.; Zhang, L.-L.; Ni, S.-B. Reduced graphene oxide decorated ternary Cu_2SnS_3 as anode materials for lithium ion batteries. *J. Electroanal. Chem.* **2016**, *760*, 127–134. [CrossRef]
22. Maheskumar, V.; Sheebha, I.; Vidhya, B.; Deebasree, J.P.; Selvaraju, T.; Akash, S. Enhanced electrocatalytic and photocatalytic activity of ball milled copper tin sulphide by incorporating GO and RGO. *Appl. Surf. Sci.* **2019**, *484*, 265–275. [CrossRef]
23. Yao, S.; Xu, L.; Gao, Q.; Wang, X.; Kong, N.; Li, W.; Wang, J.; Li, G.; Pu, X. Enhanced photocatalytic degradation of rhodamine b by reduced graphene oxides wrapped-Cu_2SnS_3 flower-like architectures. *J. Alloys Compd.* **2017**, *704*, 469–477. [CrossRef]
24. Machale, A.R.; Phaltane, S.A.; Shelke, H.D.; Kadam, L.D. Facile hydrothermal synthesis of Cu_2SnS_3 nanoparticles for photocatalytic dye degredation of mythelene blue. *Mater. Today Proc.* **2021**, *43*, 2768–2773. [CrossRef]
25. Machale, A.R.; Shelke, H.D.; Phaltane, S.A.; Kadam, L.D. Influence of hydrothermal temperature on the structural, morphological, optical and photocatalytic properties of ternary Cu_2SnS_3 nanoparticles. *Chem. Phys. Lett.* **2022**, *808*, 140097. [CrossRef]
26. Zhang, J.; Xiong, Z.; Zhao, X.S. Graphene-metal-oxide composites for the degradation of dyes under visible light irradiation. *J. Mater. Chem.* **2011**, *21*, 3634–3640. [CrossRef]
27. Gao, P.; Liu, J.; Sun, D.D.; Ng, W. Graphene oxide-CdS composite with high photocatalytic degradation and disinfection activities under visible light irradiation. *J. Hazard. Mater.* **2013**, *250–251*, 412–420. [CrossRef]
28. Padmanabhan, N.T.; Thomas, N.; Louis, J.; Mathew, D.T.; Ganguly, P.; John, H.; Pillai, S.C. Graphene coupled TiO_2 photocatalysts for environmental applications: A review. *Chemosphere* **2021**, *271*, 129506. [CrossRef]

Disclaimer/Publisher's Note: The statements, opinions and data contained in all publications are solely those of the individual author(s) and contributor(s) and not of MDPI and/or the editor(s). MDPI and/or the editor(s) disclaim responsibility for any injury to people or property resulting from any ideas, methods, instructions or products referred to in the content.